CHEMISTRY OF MATERIALS

pubs.acs.org/cm

Article

# Defect Engineering in Epitaxial Thin Films of the Pyrochlore Frustrated Magnet $Tb_2Ti_2O_7$

Margaret A. Anderson, Ismail El Baggari, Charles M. Brooks, Troy Powell, Chris Lygouras, Alpha T. N'Diaye, Seyed M. Koohpayeh, Johanna Nordlander,* and Julia A. Mundy*

Cite This: *Chem. Mater.* 2024, 36, 2325−2333

Read Online

ACCESS | Metrics & More | Article Recommendations | Supporting Information



**ABSTRACT:** Among the pyrochlore oxides, the frustrated magnet $Tb_2Ti_2O_7$ has drawn intense interest as a spin liquid candidate. Its unusual magnetic properties rely on a careful balance of interactions on the frustrated pyrochlore lattice and are exquisitely sensitive to composition. Leveraging the precise stoichiometry control of reactive-oxide molecular beam epitaxy, we manipulate the defect chemistry of $Tb_2Ti_2O_7$ thin films on (111)-oriented YSZ substrates and probe their structural and magnetic properties. Single-phase pyrochlore thin films are realized within a large growth window at up to 25% off-composition. Using both scanning transmission electron microscopy and electron energy loss spectroscopy, we demonstrate the preferential formation of distinct defects with varying film stoichiometry. Titanium-rich films incorporate titanium excess via antistuffing of both $Ti^{3+}$ and $Ti^{4+}$ locally along slanted $\langle 11\bar{2} \rangle$ antiphase boundaries. In contrast, excess terbium is directly incorporated into the film through homogeneous stuffing and terbium-rich films exhibit mostly $\langle 111 \rangle$ antiphase boundaries. DC magnetic susceptibility measurements suggest that defects reduce the frustration index of $Tb_2Ti_2O_7$, with titanium and terbium excess both leading to an enhanced saturated magnetic moment and less negative Curie−Weiss temperature compared to the stoichiometric film, while all films remain paramagnetic down to 1.8 K.

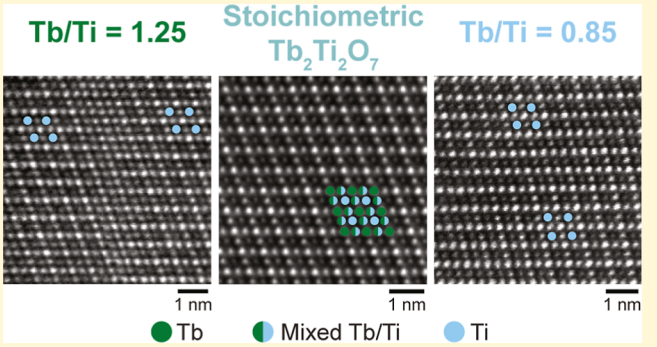


## INTRODUCTION

The pyrochlore oxides ($A_2B_2O_7$, $A$, $B$ = cations) form a large class of materials with ground states that include topological insulators, ferromagnetic insulators, spin glasses, and quantum spin liquid candidates.[1−6] They are used in applications ranging from solid oxide fuel cells[7] to the immobilization of nuclear waste material.[8] Among the pyrochlores, the rare-earth titanates, $R_2Ti_2O_7$ with $R$ = Sm−Lu or Y, have attracted considerable interest in the past few decades, stemming from their unique and varied magnetic behavior.[9−11] The rare-earth $A$-site ions can possess magnetic moments with symmetries ranging from fully three-dimensional Heisenberg spins to Ising spins symmetrically constrained to lie along the local $\langle 111 \rangle$ directions. The rare-earth cations' large, localized moments lead to magnetic dipole interactions on the same energy scale as direct exchange which contribute to magnetic frustration. Cations in the pyrochlore lattice form networks of corner-sharing tetrahedra that host geometric frustration (Figure 1a). Along the $\langle 111 \rangle$ direction, each cation forms alternating Kagomé and triangular lattice layers corresponding to the interconnected bases and apexes of the tetrahedra (Figure 1b). Both antiferromagnetic Heisenberg spins and ferromagnetic Ising spins are predicted to be highly frustrated on this pyrochlore sublattice.[9] For example, $Gd_2Ti_2O_7$, with a net antiferromagnetic coupling between Heisenberg spins, exhibits partial ordering at around 1 K.[12] Similarly frustrated, $Dy_2Ti_2O_7$ and $Ho_2Ti_2O_7$ host ferromagnetic Ising spins and are considered "spin ices", which are a type of classical spin liquid with frustration analogous to the ordering of hydrogen bonds in water ice.[13−15]

$Tb_2Ti_2O_7$ stands out among the rare-earth titanate family as an enduring enigma. Its Ising spins[16,17] with net antiferromagnetic coupling should exhibit a long-range all-in-all-out ordering transition at 1−2 K.[18,19] Bulk crystals, however, show no signs of magnetic ordering down to at least 50 mK.[20,21] This unexpected behavior has fueled two decades of interest in $Tb_2Ti_2O_7$ and related pyrochlores. Leading hypotheses suggest that the non-Ising character of low lying excited crystal field states leads to transverse magnetic fluctuations which suppress long-range order.[18,19,22,23] Additionally, $Tb_2Ti_2O_7$ may lie near a quantum critical point between the all-in-all-out ordered state

Received: October 11, 2023
Revised: February 5, 2024
Accepted: February 6, 2024
Published: February 23, 2024

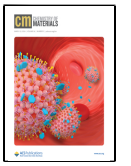

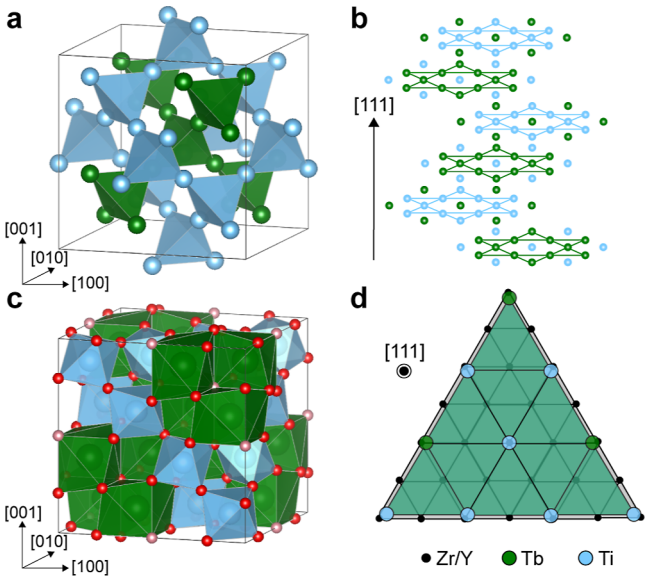


**Figure 1.** Crystal structure of $Tb_2Ti_2O_7$. Terbium atoms, titanium atoms, and oxygen atoms are shown as green, blue, and red or pink, respectively. (a) Interpenetrating pyrochlore sublattices of the terbium and titanium cations are shown with emphasized local tetrahedra within a unit cell of $Tb_2Ti_2O_7$. (b) Alternating layers of Kagomé and triangular lattices of the cations in the ⟨111⟩ direction of the pyrochlore structure. One unit cell contains six unique stacking layers in this direction. (c) Full cubic unit cell of $Tb_2Ti_2O_6O'$ with terbium atoms and their coordination polyhedra in green, titanium atoms in blue, O-site oxygen atoms in red, and the symmetrically distinct O′-site oxygen atoms in pink. (d) Illustration of the lattice matching between bulk $Tb_2Ti_2O_7$ ($a$ = 10.15 Å[32,33,46]) and the (111)-oriented YSZ substrate ($a$ = 5.14 Å). The lattice mismatch between $Tb_2Ti_2O_7$ and double the YSZ lattice parameter is 1.3%.

and the spin ice state which would lead to quantum spin fluctuations.[22] Overall, $Tb_2Ti_2O_7$ seems to behave much like a quantum spin ice,[24,25] the quantum analogue of a classical spin ice, though it does not host the ferromagnetically coupled Ising spins with perturbative transverse spin fluctuations proposed as building blocks for the quantum spin ice state.[26] Instead, $Tb_2Ti_2O_7$ has antiferromagnetic interactions and may have magnetoelastic coupling that further complicates its ground-state behavior.[27,28] In all, $Tb_2Ti_2O_7$ remains an intriguing material and one of the most enduring pyrochlore quantum spin liquid candidates.

The unusual magnetic behavior of $Tb_2Ti_2O_7$ relies on a careful balance of magnetic interactions on a perfect crystal lattice. Crystalline defects disrupt this balance.[29,30] The chemical formula for pyrochlore oxides is $A_2B_2O_7$, or more accurately $A_2B_2O_6O'$, where $A$ and $B$ are cations with oxidation states +3 and +4 (in some cases, +2 and +5), respectively. O and O′ represent two crystallographically distinct oxygen sites in the structure (Figure 1c).[29] The 8-fold-coordinated $A$-site cation lies in a highly distorted coordination configuration called a scalenohedron.[31] Composed of a rumpled ring of six oxygen atoms and two more distant apical O′ sites, the local $A$-site crystal field symmetry is strongly axial.[11] The non-Kramers ion $Tb^{3+}$, with an even number of $f$-shell electrons, is especially susceptible to distortions of its local crystal field environment. Disruption of the local symmetry could even lead to a nonmagnetic ground state, impeding the understanding of the true ground-state magnetic behavior of $Tb_2Ti_2O_7$.[11] Studies of bulk materials have shown that changes in the terbium or titanium content as little as 0.5% can lead to a detectable magnetic transition at low temperature.[32,33] Other pyrochlores have also exhibited an acute sensitivity to defects, showing changes in not only their magnetic behavior but also ionic conductivity and durability for nuclear waste storage.[7,8,11,34−40] The most common and well-studied defects in the pyrochlore lattice are oxygen vacancies and cation disorder.[34,36,41−43] These defects often coexist in pyrochlores because the positive charge of an oxygen vacancy can be balanced by "stuffing" an $A^{3+}$ ion on the $B^{4+}$ site. Furthermore, both terbium and titanium can be stabilized in either a +3 or a +4 oxidation state. Therefore, depending on synthesis conditions, $Tb_2Ti_2O_7$ could exhibit cation site substitution, changes in oxygen stoichiometry, and modified cation oxidation states.

In this paper, we synthesize thin films of the rare-earth titanate pyrochlore $Tb_2Ti_2O_7$[44,45] with molecular beam epitaxy (MBE) and characterize their structural and magnetic properties. We demonstrate control over the defect chemistry in $Tb_2Ti_2O_7$ thin films by tuning their stoichiometry. We provide a survey of the various defects that preferentially form in stoichiometric and off-composition $Tb_2Ti_2O_7$ films and present atomic resolution high-angle annular dark field scanning transmission electron microscopy (HAADF-STEM) and electron energy loss spectroscopy (EELS) that show chemical changes around these defects. This analysis provides both an insight into the formation of off-composition pyrochlores and a microscopic look at how defects may lead to changes in the magnetic behavior of $Tb_2Ti_2O_7$ and related materials.

## EXPERIMENTAL SECTION

Using reactive-oxide MBE, we synthesized epitaxial thin films of $Tb_{2+x}Ti_{2-x}O_{7\pm\delta}$ on (111)-oriented yttria-stabilized zirconia (YSZ) substrates (CrysTec GmbH). Prior to deposition, we sonicated the YSZ substrates in acetone, isopropyl alcohol, and deionized water before annealing in air at 1300 °C for 3 h to achieve ideal atomically flat, stepped surfaces (Supporting Information Figure S1).[47] We calibrated the terbium metal flux by extracting the thickness of $Tb_2O_3$ films from X-ray reflectivity measurements and derived a tooling factor based on flux measured with a quartz crystal microbalance (QCM).[48] We determined the titanium flux from in situ reflection high-energy electron diffraction (RHEED) intensity oscillations during shuttered synthesis of $SrTiO_3$. With simultaneous deposition of both cations (codeposition), we synthesized high-quality $Tb_2Ti_2O_7$ films with terbium to titanium cation ratios ranging from 25% terbium excess (Tb/Ti = 1.25) to nearly 20% excess titanium (Tb/Ti = 0.85). The film composition was verified postsynthesis via Rutherford back scattering. Films were also produced via solid-phase epitaxy (Supporting Information Figure S2) with similar crystal quality but a rough film surface.

In situ RHEED provided a real-time indication of the crystallinity and surface morphology of the films during synthesis. We produced smooth, highly crystalline pyrochlore films over a wide range of synthesis conditions: with substrate temperature ranging from 650 to 850 °C, measured by an infrared pyrometer focused on a platinum coating on the back of the substrates, and in oxygen environments ranging from $10^{-6}$ Torr $O_2$ to $5 \times 10^{-7}$ Torr distilled $O_3$ supplied by a Heeg Vacuum Engineering ozone distillation system. A temperature of 800 °C in $10^{-6}$ Torr of 10% $O_3/O_2$ led to the highest quality films as characterized by RHEED and X-ray diffraction (XRD). All $Tb_2Ti_2O_7$ films discussed below were synthesized at these ideal conditions with a thickness of approximately 15 nm.

Surface topography was probed with an Asylum MFP-3D Origin atomic force microscope in tapping mode. We used a Malvern Panalytical Empyrean diffractometer with Cu−K$\alpha_1$ radiation ($\lambda$ = 1.5406 Å) and a PIXcel3D detector for X-ray diffraction, X-ray


https://doi.org/10.1021/acs.chemmater.3c02603
Chem. Mater. 2024, 36, 2325−2333

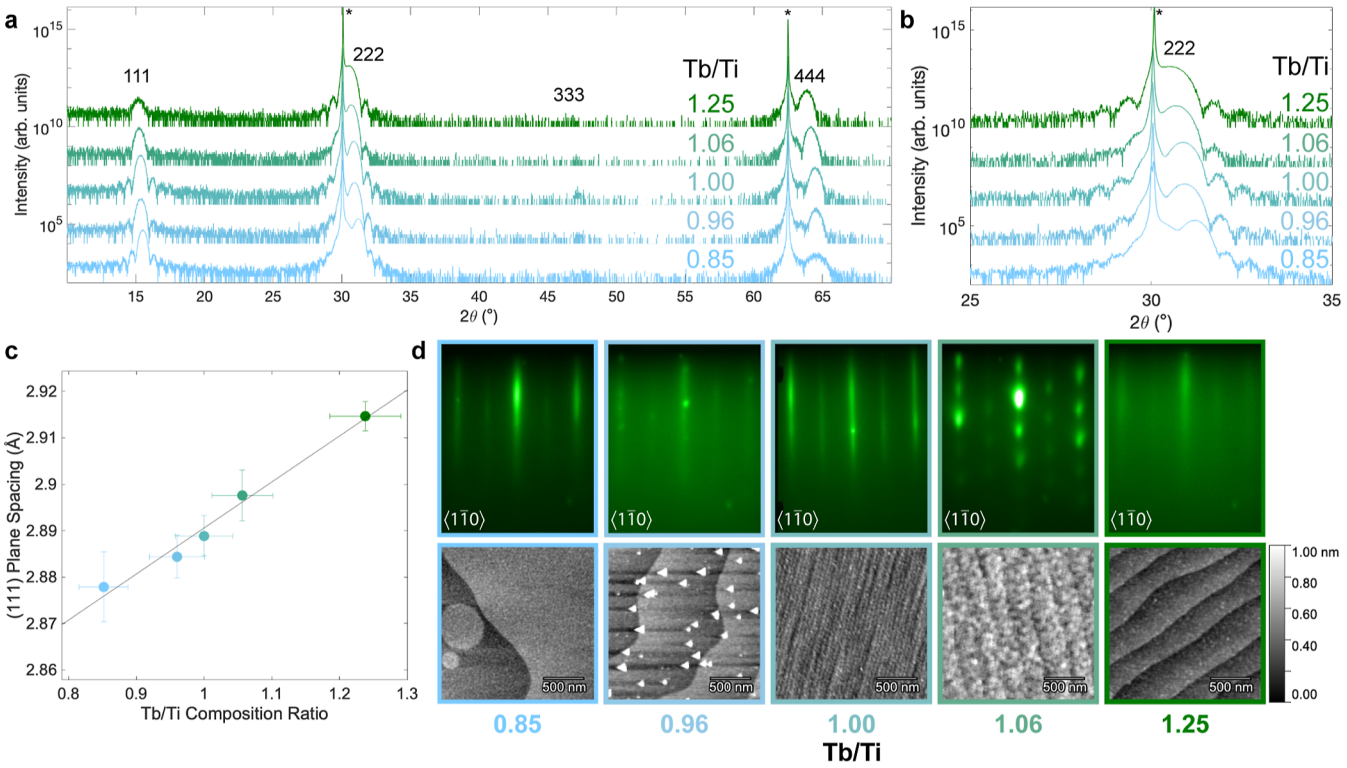


**Figure 2.** Structural characterization of $Tb_2Ti_2O_7$ thin films with varying stoichiometry. (a) XRD scans of the film series showing a slight shift in peak position with stoichiometry as well as changes in peak intensities. (b) Expanded view of the 222 peaks from the XRD patterns demonstrating an increasing lattice parameter with more terbium. (c) Film (111) plane spacing extracted from Nelson−Riley fitting of the XRD peak positions shows a linear trend with cation stoichiometry. (d) Varying surface morphology of the film series probed by in situ RHEED (top row) and atomic force microscopy (AFM) (bottom row).

reflectivity, and reciprocal space mapping. We extracted an estimated (111) atomic plane spacing for each film from the Nelson−Riley extrapolation method.[49]

We measured the magnetic properties with a Quantum Design Magnetic Property Measurement System. To correct for the large and varied magnetic background contributed by paramagnetic impurities in the otherwise diamagnetic YSZ substrates, we measured the magnetic moment of the film and substrate system and then subtracted the corresponding moment of each bare substrate measured after removing the film.

We collected X-ray absorption spectra in total electron yield mode at beamline 6.3.1 at the Advanced Light Source at Lawrence Berkeley National Laboratory (Supporting Information Figure S3).

We produced lamellae for cross-sectional STEM imaging with an FEI Helios 660 focused ion beam system and performed preliminary imaging on a JEOL ARM 200F STEM at 200 kV. Final imaging and EELS measurements were collected on a Thermo Fisher Scientific Themis Z G3 aberration-corrected STEM operating at 200 kV with an 18.9 mrad convergence angle and a collection angle ranging from 72 to 200 mrad. Stacks of short exposure images were cross-correlated and averaged to correct for beam instabilities and drift. Atomic resolution EELS maps were captured with a Gatan Continuum detector with a dispersion of 0.15 eV and 10 ms dwell time. Background subtracted maps were processed with local background averaging to improve the signal-to-noise ratio.[50]

## RESULTS

A series of five $Tb_2Ti_2O_7$ thin films with terbium to titanium composition ratios ranging from 0.85 to 1.25 form the core data set for this composition study. Across the entire series, the films are highly crystalline with Laue oscillations around the 111 and 222 X-ray diffraction peaks (Figure 2a). The series shows a slight decrease in 111 peak intensity, indicative of a loss of structural order—especially out-of-plane stacking, with excess terbium content and little to no loss of intensity for films with excess titanium. Mullens et al. see a similar loss of pyrochlore superlattice peak intensity in stuffed (ytterbium-rich) $Yb_2Ti_2O_7$.[36] Figure 2b shows a shifting of the 222 diffraction peaks to higher (lower) angles with increasing titanium (terbium) content. Extracted from Nelson−Riley fitting, the (111) plane spacing of the films shows a linear correlation with composition, where the spacing grows with the incorporation of additional terbium due to its larger ionic radii (Figure 2c). Similar trends are reported for powder, polycrystalline, and bulk single-crystal synthesis of $Tb_2Ti_2O_7$.[32,33,42,46,51]

Bulk crystals of $Tb_2Ti_2O_7$ have a 1.3% lattice mismatch with twice the lattice parameter of YSZ (Figure 1d). Reciprocal space mapping shows that all of the 15 nm films are almost fully strained to the substrate, with a weak diffuse relaxed background (Supporting Information Figure S4a). $\omega$-Rocking curves provide further evidence that the films are largely strained to the substrate: the film peaks are sharp with a substrate-limited full width at half-maximum (FWHM) and a weak broad background that accompanies partial relaxation (Supporting Information Figure S5b). Furthermore, the (111) plane spacing of the films is smaller than in bulk samples, as expected with tensile strain.

From in situ RHEED captured at the end of each growth (top row Figure 2d), we conclude that $Tb_2Ti_2O_7$ forms as a single-phase solid solution with the exception of small amounts of excess titanium that form triangular $TiO_x$ islands on top of an otherwise smooth film surface. The stoichiometric film appears to be highly crystalline and well ordered. AFM


https://doi.org/10.1021/acs.chemmater.3c02603
Chem. Mater. 2024, 36, 2325−2333

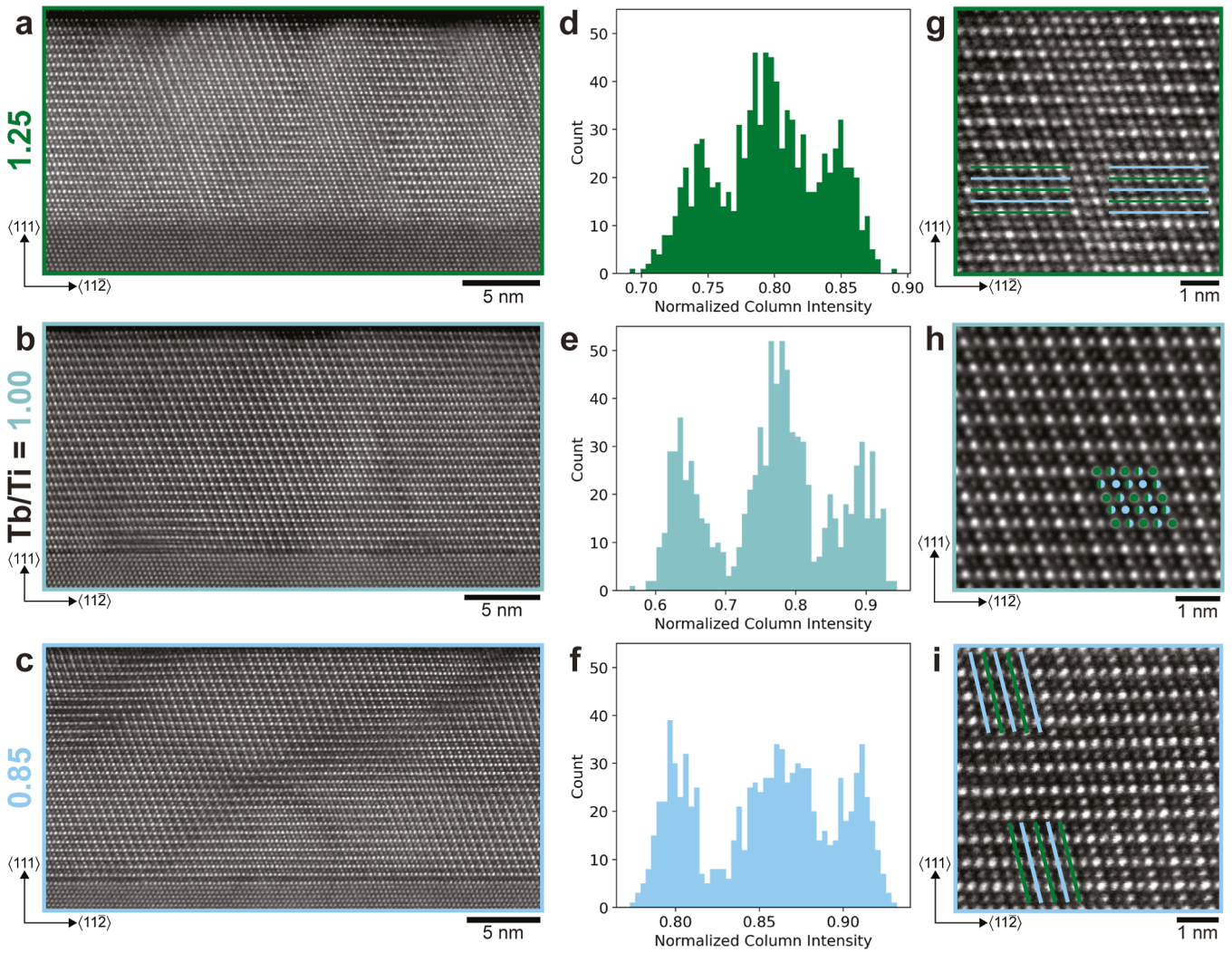


**Figure 3.** HAADF-STEM imaging of the $Tb_2Ti_2O_7$ film series. (a–c) HAADF micrographs of the Tb-rich (a), stoichiometric (b), and Ti-rich (c) $Tb_2Ti_2O_7$ films on YSZ(111) imaged along ⟨1$\bar{1}$0⟩ (low magnification presented in Supporting Information Figure S8). (d–f) Histograms of the normalized intensity of the atomic columns mapped out using Gaussian fitting from largely defect-free regions of the films in (a–c) ($n \approx 940$, see Supporting Information Figure S9 for details). (g–i) Higher magnification HAADF micrographs of (g) a ⟨111⟩ antiphase boundary typical in the Tb-rich film, green (blue) lines indicate terbium (titanium) Kagomé planes; (h) the ideal checkerboard pyrochlore contrast in the stochiometric film, green dots denote pure terbium columns, blue denote pure titanium, and half-blue–half-green indicate mixed occupancy columns composed of alternating terbium and titanium atoms; and (i) a ⟨11$\bar{2}$⟩-oriented antiphase boundary common in the Ti-rich film.

(bottom row Figure 2d) shows that the film is exceptionally smooth with an RMS surface roughness of about 100 pm. Slight excess terbium results in a modulated film surface indicated by the spotted RHEED and increased surface roughness of 140 pm. With 25% excess terbium (Tb/Ti = 1.25), the RHEED streaks become wider and more diffuse, indicating a loss of crystalline quality. Nevertheless, the surface of the film remains remarkably smooth as measured in AFM with a roughness similar to the stoichiometric film. For Tb/Ti = 0.96, the formation of $TiO_x$ islands is accompanied by a broadening of the RHEED pattern. In contrast, 20% titanium excess (Tb/Ti = 0.85) is fully incorporated into the film, resulting in a smooth surface topography and sharp, intense RHEED streaks with less prominent half-order than the stoichiometric sample.

In Figure 3, we present HAADF-STEM imaging of the local microstructure for three films with a terbium to titanium ratio of 1.25 (Figure 3a), 1.00 (Figure 3b), and 0.85 (Figure 3c). The stoichiometric $Tb_2Ti_2O_7$ film (Figure 3b,e,h) exhibits large regions of checkerboard contrast indicative of a well-ordered pyrochlore structure (Figure 3h). Occasionally, an additional (11$\bar{1}$) plane of $Tb_2Ti_2O_7$ occurs as a dislocation along the substrate–film interface to locally relax the tensile strain. One such dislocation is visible in the large field-of-view HAADF image (Figure 3b) as a region with a loss of atomic resolution and of the ⟨11$\bar{2}$⟩ alternating contrast (Supporting Information Figure S12). The terbium-rich film with Tb/Ti = 1.25 (Figure 3a,d,g) has small well-ordered regions interrupted by several ⟨111⟩-oriented antiphase boundaries as highlighted in Figure 3g. In contrast, the titanium-rich film with Tb/Ti = 0.85 (Figure 3c,f,i) hosts mainly ⟨11$\bar{2}$⟩-oriented antiphase boundaries. Because the antiphase boundaries must terminate at the edge of the crystal or at a dislocation, they slant upward and extend between the interface and film surface. Figure 3i shows that the ⟨11$\bar{2}$⟩ antiphase boundaries are accompanied by a region without clear pyrochlore contrast, indicative of cation disorder (Supporting Information Figure S13).


https://doi.org/10.1021/acs.chemmater.3c02603
Chem. Mater. 2024, 36, 2325−2333

Analysis of the distribution of atomic column intensity projected along ⟨1$\bar{1}$0⟩ in the stoichiometric, titanium-rich, and terbium-rich films (Figure 3d–f) shows that the stoichiometric film (Figure 3e) has three distinct intensity values corresponding to the three types of atomic columns in the pyrochlore structure (pure terbium, pure titanium, and an equal mixture). The intensity distribution of the titanium-rich film (Figure 3f) is qualitatively similar, but with reduced separation between the terbium and mixed columns possibly indicating antistuffing of titanium on the terbium sites. The terbium-rich film (Figure 3d) shows a less clear distinction between all three intensity values, suggesting widespread cation disorder and stuffing. The intensity of atomic columns in HAADF images corresponds to the atomic number of the atoms in that column. Reduced separation between the intensities of the brightest (pure terbium) and the middle intensity (mixed) columns in the titanium-rich film suggests that the intensity of the terbium columns may have been reduced by the presence of some titanium via antistuffing. Equivalently, the intensity values of the terbium-rich film may be less distinct due to excess terbium occupying titanium sites in the titanium and mixed columns and causing increased column intensities.

Atomic resolution electron energy loss spectroscopy (EELS) of the antiphase boundaries within the off-composition films reveals several important differences between the defects in titanium- and terbium-rich films. In the film with excess titanium (Figure 4), EELS mapping around an antiphase boundary shows a higher concentration of titanium localized to the defect (Figure 4b). Multivariate curve resolution (MCR) analysis[52] identifies two distinct titanium EELS fingerprints around the defect (Figure 4d,e). In regions with clear pyrochlore order away from the boundary, the titanium $L_{2,3}$ edge exhibits the expected four-peaked structure of $Ti^{4+}$ with nearly octahedral coordination.[53] Within the region surrounding the antiphase boundary, the titanium edge shifts to lower energy and the four peaks merge into two, indicating a reduction of the titanium ions toward $Ti^{3+}$ and a change in local crystal symmetry suggestive of cation disorder.[53] The reduction coupled with a change in coordination symmetry in the region of excess titanium provides strong evidence of antistuffing, where extra titanium occupies the 8-fold-coordinated *A*-site as $Ti^{3+}$ to maintain a neutral charge within the structure without excess oxygen. EELS mapping around other antiphase boundaries in the same sample also shows regions of $Ti^{4+}$ with a modified EELS spectra coincident with a region of excess oxygen, suggesting that titanium may be antistuffed as $Ti^{4+}$ as well (Supporting Information Figure S7). $Ti^{3+}$ and $Ti^{4+}$ are not expected to be stable on the *A*-site in an otherwise pristine pyrochlore lattice. However, regions of the crystal with disrupted symmetry around defects, such as antiphase boundaries, may accommodate antistuffing of titanium on the terbium site. Separate maps of the MCR component concentrations show that within the antiphase boundary, ideal octahedrally coordinated $Ti^{4+}$ on the *B*-site only persists in small amounts in (111) titanium Kagomé planes where proper pyrochlore stacking is preserved (Supporting Information Figure S6). Some studies of bulk pyrochlore crystals suggest that antistuffing of $Ti^{4+}$ may occur in highly disordered samples.[36,40,54] Ghasemi et al.[35] find that antistuffing occurs in their titanium-rich $Ho_2Ti_2O_7$ powders,

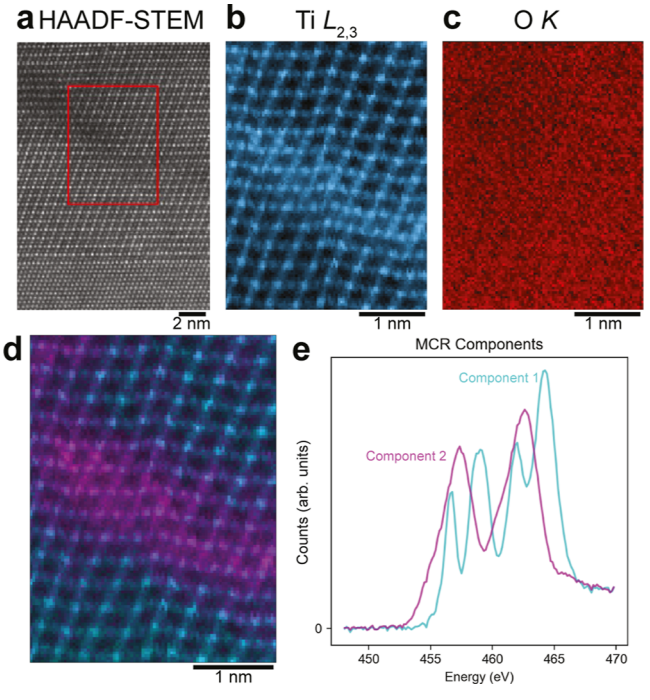


**Figure 4.** Atomic resolution electron energy loss spectroscopy (EELS) of antiphase boundaries in a titanium-rich $Tb_2Ti_2O_7$ thin film. (a) HAADF-STEM survey image with the region of interest around a ⟨11$\bar{2}$⟩ antiphase boundary indicated in red. (b) Titanium $L_{2,3}$ edge EELS concentration map. (c) Oxygen *K* edge EELS concentration map. (d) Score map of the two component edges derived from MCR analysis of the titanium $L_{2,3}$ edge. (e) Plot of the two titanium $L_{2,3}$ edge components identified with MCR.

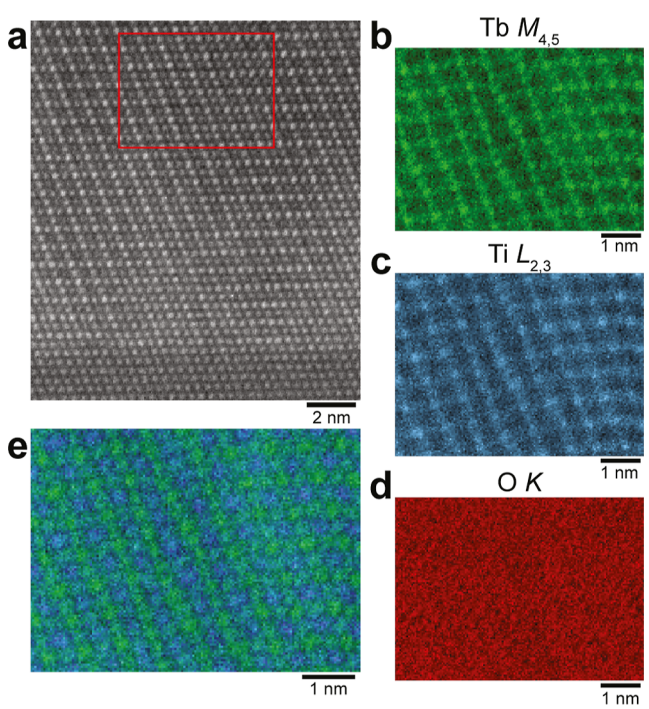


**Figure 5.** Atomic resolution electron energy loss spectroscopy (EELS) of antiphase boundaries in a terbium-rich $Tb_2Ti_2O_7$ thin film. (a) A HAADF-STEM survey image with the region of interest (indicated in red) around a vertical ⟨111⟩ antiphase boundary. (b–d) EELS elemental concentration maps for terbium (b), titanium (c), and oxygen (d) in the region of interest. (e) Composite color map of the local concentration of terbium (green) and titanium (blue).


https://doi.org/10.1021/acs.chemmater.3c02603
Chem. Mater. 2024, 36, 2325−2333

but only for high synthesis temperatures (1500 °C). At lower temperatures, they find that the excess titanium forms $TiO_2$. In our films, low amounts of titanium excess (Tb/Ti = 0.96) appear to precipitate out as oxide islands while larger titanium excess (Tb/Ti = 0.85) leads to antistuffing localized to defects such as antiphase boundaries.

In stark contrast, the terbium-rich film (Figure 5) shows a homogeneous distribution of terbium, titanium, and oxygen with no clear excess or deficiency within an antiphase boundary (Figure 5b–d). MCR processing failed to identify multiple spatially resolved EELS edges across the defect which suggests that either each element has a consistent oxidation state and coordination environment across the defect or that multiple species are uniformly distributed. The composite EELS map of terbium and titanium concentration in Figure 5e shows that there is a narrow defect region around the boundary where the checkerboard pyrochlore contrast is lost and replaced by alternating terbium and titanium-rich $(11\bar{1})$ planes without a local excess of either element. In pyrochlore crystals, the stuffing of a $Tb^{4+}$ ion on the *B*-site is expected to be stable, so this cation substitution may occur within the otherwise ideal pyrochlore structure. Considering the reduced variation in atomic column intensity in HAADF images of this terbium-rich sample with the homogeneous EELS elemental maps, we posit that terbium is uniformly stuffed within the film.

Figure 6 shows the magnetic properties of the stoichiometric and the most off-composition films in the series (for magnetic characterization of the full series, see Supporting Information Figures S10 and S11). All films remain paramagnetic down to 1.8 K as evidenced by the absence of ferromagnetic hysteresis as well as any phase transition in the temperature-dependent magnetic susceptibility (Supporting Information Figure S11). Magnetization loops at 1.8 K (Figure 6a) show that both excess terbium and titanium lead to an enhanced saturation magnetization in our films. Curie–Weiss fitting to the inverse susceptibility (Figure 6b) gives a Curie–Weiss temperature ($\theta_{CW}$) of −25 K for the stoichiometric film, similar to that in bulk samples and indicative of net antiferromagnetic interactions.[20] The measured Curie–Weiss temperature contrasted with the lack of a magnetic ordering transition above 1.8 K suggests that the films are highly frustrated like bulk crystals.[21] The off-composition films have lower magnitude Curie–Weiss temperatures (Supporting Information Figure S10), suggesting an increased noninteracting paramagnetic background or modified coupling between moments as well as a reduced frustration index $\left(f = \frac{\theta_{CW}}{T_c}\right)$. In the terbium-rich films, $Tb^{4+}$ ions stuffed onto the *B*-site may increase the connectivity of the ideal $Tb^{3+}$ lattice or contribute a new paramagnetic signal. $Ti^{4+}$ has an empty *d*-shell and is nonmagnetic, but excess titanium reduced to $Ti^{3+}$ at defects in the titanium-rich crystals likely contribute to the magnetism. Because these magnetic ions are localized to defects, they are less likely to impact the magnetic behavior of the surrounding pristine crystal and instead may contribute a paramagnetic background signal stemming from dilute magnetic ions.[30] Indeed, bulk studies find that the lack of magnetic order in $Tb_2Ti_2O_7$ persists up to a few percent of excess titanium.[11,32]

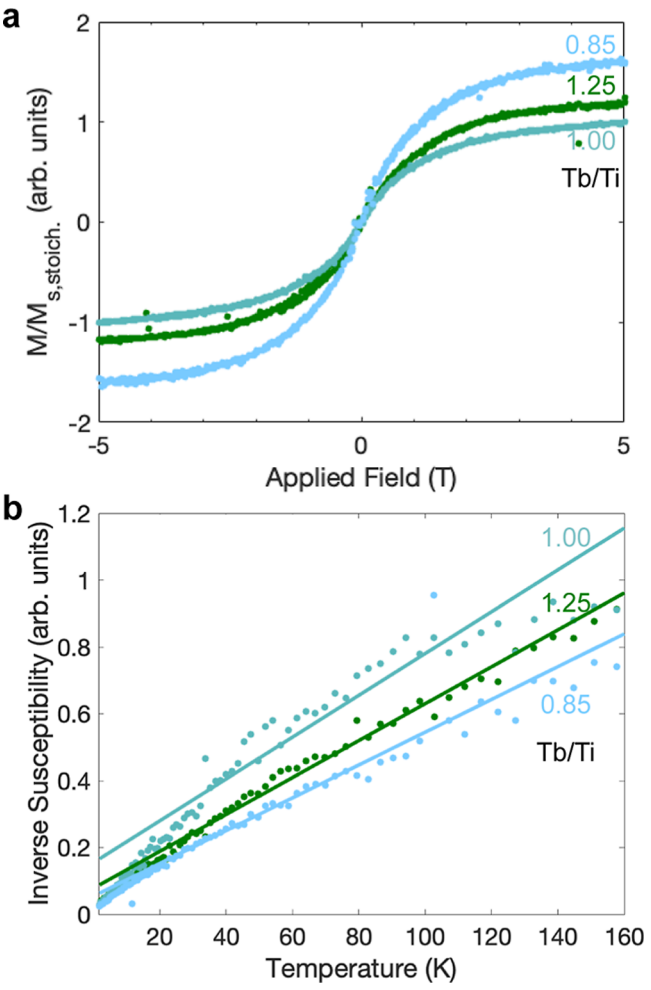


**Figure 6.** Magnetic behavior of $Tb_2Ti_2O_7$ thin films. (a) Magnetization vs applied field curves that show paramagnetic behavior taken at 1.8 K along $\langle 1\bar{1}0\rangle$ with substrate and diamagnetic contribution subtracted out, adjusted for film volume, and normalized by the maximum magnetization of the stoichiometric film. (b) Zero-field cooled inverse susceptibility measured upon warming in a 0.2 T applied field along $\langle 1\bar{1}0\rangle$. The data is corrected for substrate and diamagnetic contributions as described in Methods. Curie–Weiss fits between 20 and 150 K are plotted as solid lines. The linear fits give Curie–Weiss temperatures of −25 K (stoichiometric), −11 K (Ti-rich), and −14 K (Tb-rich).

## CONCLUSIONS

We find that $Tb_2Ti_2O_7$ is a robust crystal which forms single-phase pyrochlore thin films over a wide range of synthesis conditions and compositions. Thin films on YSZ(111) substrates exhibit a linear trend of out-of-plane (111) atomic plane spacing with composition, similar to bulk composition studies. In contrast to bulk crystals, all five films in the composition series are tensile strained to the substrate. Strain is accommodated in stoichiometric films by dislocations along the interface. In off-stoichiometry films, extended defects, especially antiphase boundaries, form preferentially both in response to the change in composition and to accommodate strain.

Excess terbium is incorporated in the films via the well-studied process of stuffing onto the *B*-site, causing an increase in surface roughness and a gradual reduction in crystalline quality associated with the formation of $\langle 111\rangle$ antiphase boundaries and cation disorder. In contrast, low levels of excess titanium precipitate out as oxide islands on the film surface while larger amounts incorporate into the film along $\langle 11\bar{2}\rangle$ antiphase boundaries via antistuffing as both $Ti^{3+}$ and $Ti^{4+}$.


https://doi.org/10.1021/acs.chemmater.3c02603
Chem. Mater. 2024, 36, 2325−2333

Though antistuffing is only rarely reported in bulk crystals, we find that, with epitaxial stabilization, $Tb_2Ti_2O_7$ thin films exhibit antistuffing along antiphase boundaries within the pyrochlore structure.

In magnetic measurements, all films remain paramagnetic down to 1.8 K, while the off-composition films exhibit enhanced saturated moments in an applied field as well as less negative Curie−Weiss temperatures. The moment enhancement likely stems from the additional magnetic $Ti^{3+}$ or $Tb^{4+}$ ions incorporated into the films. The change in the Curie−Weiss temperature suggests an added noninteracting paramagnetic background or a reduced moment coupling. The combination of a decreased Curie−Weiss temperature and persistent lack of an ordering transition down to 1.8 K effectively lowers the frustration index of the nonstoichiometric films.

Along with changes in composition, strain seems to be a driving factor of defect formation in these films. Titanium excess results in a reduced lattice parameter. The shrinking lattice constant leads to a larger lattice mismatch between the film and substrate. In response, the more highly strained titanium-rich films tend to concentrate excess titanium atoms in-plane in $\langle 11\bar{2} \rangle$ antiphase boundaries which help reduce the out-of-plane lattice constant and relieve strain (see Supporting Information Figure S5a). In terbium-rich films, $\langle 111 \rangle$ antiphase boundaries and widespread cation disorder slightly expand the in-plane lattice constant, thereby reducing the lattice mismatch with the YSZ substrate and thus reducing the strain. This preferential formation of extended defects may therefore be specific to epitaxially strained thin films of $Tb_2Ti_2O_7$. In bulk samples without the influence of strain, the formation of extended defects may have a different behavior.

Understanding the formation of defects and the accommodation of off-stoichiometry in $Tb_2Ti_2O_7$ informs the synthesis and characterization of other rare-earth titanates and members of the pyrochlore class. Pyrochlores have shown an acute sensitivity to changes in composition which affects their functionality in a variety of applications. Hence, defect engineering, as demonstrated here through thin-film epitaxy, provides a powerful route to tuning pyrochlore functionality.

## ■ ASSOCIATED CONTENT

### Supporting Information

The Supporting Information is available free of charge at https://pubs.acs.org/doi/10.1021/acs.chemmater.3c02603.

X-ray absorption spectroscopy, strain characterization and mapping, additional STEM analysis and examples, additional magnetic characterization, substrate characterization, and characterization of a film synthesized via solid-phase epitaxy (PDF)

## ■ AUTHOR INFORMATION


### Corresponding Authors

**Johanna Nordlander** − *Department of Physics, Harvard University, Cambridge, Massachusetts 02138, United States; Paul Drude Institute for Solid State Electronics, 10117 Berlin, Germany;* orcid.org/0000-0002-9899-6795; Email: nordlander@pdi-berlin.de

**Julia A. Mundy** − *Department of Physics, Harvard University, Cambridge, Massachusetts 02138, United States;* orcid.org/0000-0001-8454-0124; Email: mundy@fas.harvard.edu

### Authors

**Margaret A. Anderson** − *Department of Physics, Harvard University, Cambridge, Massachusetts 02138, United States;* orcid.org/0000-0002-0355-0994

**Ismail El Baggari** − *The Rowland Institute at Harvard, Cambridge, Massachusetts 02142, United States*

**Charles M. Brooks** − *Department of Physics, Harvard University, Cambridge, Massachusetts 02138, United States*

**Troy Powell** − *Department of Physics, Harvard University, Cambridge, Massachusetts 02138, United States*

**Chris Lygouras** − *Institute for Quantum Matter and Department of Physics and Astronomy, Johns Hopkins University, Baltimore, Maryland 21218, United States*

**Alpha T. N'Diaye** − *Advanced Light Source, Lawrence Berkeley National Lab, Berkeley, California 94720, United States*

**Seyed M. Koohpayeh** − *Institute for Quantum Matter and Department of Physics and Astronomy, Johns Hopkins University, Baltimore, Maryland 21218, United States; Department of Materials Science and Engineering and Ralph O'Connor Sustainable Energy Institute, Johns Hopkins University, Baltimore, Maryland 21218, United States*

Complete contact information is available at: https://pubs.acs.org/10.1021/acs.chemmater.3c02603


### Notes

The authors declare no competing financial interest.

## ■ ACKNOWLEDGMENTS

The authors thank H. Hijazi at the Rutgers University Laboratory of Surface Modification for assistance in Rutherford backscattering spectrometry. This work was supported by the Air Force Research Laboratory, Project Grant FA95502110429. This research used resources of the Advanced Light Source, which is a DOE Office of Science User Facility under contract no. DE-AC02-05CH11231. Electron microscopy was performed at Harvard University's Center for Nanoscale Systems, a member of the National Nanotechnology Coordinated Infrastructure Network, supported by the NSF under grant no. 2025158. Additional electron microscopy was performed at the MIT.nano facilities at the Massachusetts Institute of Technology. The work by C.L. and S.M.K. was supported as part of the Institute for Quantum Matter, an Energy Frontier Research Center funded by the U.S. Department of Energy, Office of Science, Basic Energy Sciences under Award no. DE-SC0019331. J.A.M. acknowledges support from the Packard Foundation and Gordon and Betty Moore Foundation's EPiQS Initiative, Grant GBMF6760. J.N. acknowledges support from the Swiss National Science Foundation under Project no. P2EZP2_195686.

## ■ REFERENCES

(1) Yang, B.-J.; Nagaosa, N. Emergent topological phenomena in thin films of pyrochlore iridates. *Phys. Rev. Lett.* **2014**, *112*, 246402.

(2) Kim, W. J.; Oh, T.; Song, J.; Ko, E. K.; Li, Y.; Mun, J.; Kim, B.; Son, J.; Yang, Z.; Kohama, Y.; Kim, M.; Yang, B.-J.; Noh, T. W. Strain engineering of the magnetic multipole moments and anomalous Hall effect in pyrochlore iridate thin films. *Sci. Adv.* **2020**, *6*, No. eabb1539.

(3) Ideue, T.; Onose, Y.; Katsura, H.; Shiomi, Y.; Ishiwata, S.; Nagaosa, N.; Tokura, Y. Effect of lattice geometry on magnon Hall effect in ferromagnetic insulators. *Phys. Rev. B* **2012**, *85*, 134411.

(4) Raju, N. P.; Gmelin, E.; Kremer, R. K. Magnetic-susceptibility and specific-heat studies of spin-glass-like ordering in the pyrochlore compounds $R_2Mo_2O_7$ ($R$ = Y, Sm, or Gd). *Phys. Rev. B* **1992**, *46*, 5405−5411.
(5) Sibille, R.; Lhotel, E.; Pomjakushin, V.; Baines, C.; Fennell, T.; Kenzelmann, M. Candidate quantum spin liquid in the $Ce^{3+}$ pyrochlore stannate $Ce_2Sn_2O_7$. *Phys. Rev. Lett.* **2015**, *115*, 097202.
(6) Gao, B.; Chen, T.; Tam, D. W.; Huang, C.-L.; Sasmal, K.; Adroja, D. T.; Ye, F.; Cao, H.; Sala, G.; Stone, M. B.; et al. Experimental signatures of a three-dimensional quantum spin liquid in effective spin-1/2 $Ce_2Zr_2O_7$ pyrochlore. *Nat. Phys.* **2019**, *15*, 1052−1057.
(7) Anantharaman, A. P.; Dasari, H. P. Potential of pyrochlore structure materials in solid oxide fuel cell applications. *Ceram. Int.* **2021**, *47*, 4367−4388.
(8) Ewing, R. C.; Weber, W. J.; Lian, J. Nuclear waste disposal—Pyrochlore ($A_2B_2O_7$): Nuclear waste form for the immobilization of plutonium and "minor" actinides. *J. Appl. Phys.* **2004**, *95*, 5949−5971.
(9) Gardner, J. S.; Gingras, M. J. P.; Greedan, J. E. Magnetic pyrochlore oxides. *Rev. Mod. Phys.* **2010**, *82*, 53−107.
(10) Greedan, J. E. Frustrated rare earth magnetism: Spin glasses, spin liquids and spin ices in pyrochlore oxides. *J. Alloys Compd.* **2006**, *408*−*412*, 444−455.
(11) Rau, J. G.; Gingras, M. J. P. Frustrated quantum rare-earth pyrochlores. *Annu. Rev. Condens. Matter Phys.* **2019**, *10*, 357−386.
(12) Paddison, J. A. M.; Ehlers, G.; Cairns, A. B.; Gardner, J. S.; Petrenko, O. A.; Butch, N. P.; Khalyavin, D. D.; Manuel, P.; Fischer, H. E.; Zhou, H.; Goodwin, A. L.; Stewart, J. R. Suppressed-moment 2-**k** order in the canonical frustrated antiferromagnet $Gd_2Ti_2O_7$. *npj Quantum Mater.* **2021**, *6*, No.99.
(13) Harris, M. J.; Bramwell, S. T.; McMorrow, D. F.; Zeiske, T.; Godfrey, K. W. Geometrical frustration in the ferromagnetic pyrochlore $Ho_2Ti_2O_7$. *Phys. Rev. Lett.* **1997**, *79*, 2554−2557.
(14) Ramirez, A. P.; Hayashi, A.; Cava, R. J.; Siddharthan, R.; Shastry, B. S. Zero-point entropy in 'spin ice'. *Nature* **1999**, *399*, 333−335.
(15) Bramwell, S. T.; Gingras, M. J. P. Spin ice state in frustrated magnetic pyrochlore materials. *Science* **2001**, *294*, 1495−1501.
(16) Gingras, M. J. P.; den Hertog, B. C.; Faucher, M.; Gardner, J. S.; Dunsiger, S. R.; Chang, L. J.; Gaulin, B. D.; Raju, N. P.; Greedan, J. E. Thermodynamic and single-ion properties of $Tb^{3+}$ within the collective paramagnetic-spin liquid state of the frustrated pyrochlore antiferromagnet $Tb_2Ti_2O_7$. *Phys. Rev. B* **2000**, *62*, 6496−6511.
(17) Rosenkranz, S.; Ramirez, A. P.; Hayashi, A.; Cava, R. J.; Siddharthan, R.; Shastry, B. S. Crystal-field interaction in the pyrochlore magnet $Ho_2Ti_2O_7$. *J. Appl. Phys.* **2000**, *87*, 5914−5916.
(18) Kao, Y.-J.; Enjalran, M.; Del Maestro, A.; Molavian, H. R.; Gingras, M. J. P. Understanding paramagnetic spin correlations in the spin-liquid pyrochlore $Tb_2Ti_2O_7$. *Phys. Rev. B* **2003**, *68*, 172407.
(19) Enjalran, M.; Gingras, M. J. P.; Kao, Y.-J.; Del Maestro, A.; Molavian, H. R. The spin liquid state of the $Tb_2Ti_2O_7$ pyrochlore antiferromagnet: a puzzling state of affairs. *J. Phys.: Condens. Matter* **2004**, *16*, S673−S678.
(20) Gardner, J. S.; Dunsiger, S. R.; Gaulin, B. D.; Gingras, M. J. P.; Greedan, J. E.; Kiefl, R. F.; Lumsden, M. D.; MacFarlane, W. A.; Raju, N. P.; Sonier, J. E.; Swainson, I.; Tun, Z. Cooperative paramagnetism in the geometrically frustrated pyrochlore antiferromagnet $Tb_2Ti_2O_7$. *Phys. Rev. Lett.* **1999**, *82*, 1012−1015.
(21) Gardner, J. S.; Keren, A.; Ehlers, G.; Stock, C.; Segal, E.; Roper, J. M.; Fåk, B.; Stone, M. B.; Hammar, P. R.; Reich, D. H.; Gaulin, B. D. Dynamic frustrated magnetism in $Tb_2Ti_2O_7$ at 50 mK. *Phys. Rev. B* **2003**, *68*, 180401.
(22) Molavian, H. R.; Gingras, M. J. P. Proposal for a [111] magnetization plateau in the spin liquid state of $Tb_2Ti_2O_7$. *J. Phys.: Condens. Matter* **2009**, *21*, 172201.
(23) Gaulin, B. D.; Gardner, J. S.; McClarty, P. A.; Gingras, M. J. P. Lack of evidence for a singlet crystal-field ground state in the magnetic pyrochlore $Tb_2Ti_2O_7$. *Phys. Rev. B* **2011**, *84*, 140402.
(24) Fennell, T.; Kenzelmann, M.; Roessli, B.; Haas, M. K.; Cava, R. J. Power-law spin correlations in the pyrochlore antiferromagnet $Tb_2Ti_2O_7$. *Phys. Rev. Lett.* **2012**, *109*, 017201.
(25) Fritsch, K.; Ross, K. A.; Qiu, Y.; Copley, J. R. D.; Guidi, T.; Bewley, R. I.; Dabkowska, H. A.; Gaulin, B. D. Antiferromagnetic spin ice correlations at (1/2, 1/2, 1/2) in the ground state of the pyrochlore magnet $Tb_2Ti_2O_7$. *Phys. Rev. B* **2013**, *87*, 094410.
(26) Gingras, M. J. P.; McClarty, P. A. Quantum spin ice: A search for gapless quantum spin liquids in pyrochlore magnets. *Rep. Prog. Phys.* **2014**, *77*, 056501.
(27) Fennell, T.; Kenzelmann, M.; Roessli, B.; Mutka, H.; Ollivier, J.; Ruminy, M.; Stuhr, U.; Zaharko, O.; Bovo, L.; Cervellino, A.; Haas, M. K.; Cava, R. J. Magnetoelastic excitations in the pyrochlore spin liquid $Tb_2Ti_2O_7$. *Phys. Rev. Lett.* **2014**, *112*, 017203.
(28) Ruff, J. P. C.; Gaulin, B. D.; Castellan, J. P.; Rule, K. C.; Clancy, J. P.; Rodriguez, J.; Dabkowska, H. A. Structural fluctuations in the spin-liquid state of $Tb_2Ti_2O_7$. *Phys. Rev. Lett.* **2007**, *99*, 237202.
(29) Sala, G.; Gutmann, M. J.; Prabhakaran, D.; Pomaranski, D.; Mitchelitis, C.; Kycia, J. B.; Porter, D. G.; Castelnovo, C.; Goff, J. P. Vacancy defects and monopole dynamics in oxygen-deficient pyrochlores. *Nat. Mater.* **2014**, *13*, 488−493.
(30) Chamorro, J. R.; McQueen, T. M.; Tran, T. T. Chemistry of quantum spin liquids. *Chem. Rev.* **2021**, *121*, 2898−2934.
(31) McCauley, R. A. Structural characteristics of pyrochlore formation. *J. Appl. Phys.* **1980**, *51*, 290−294.
(32) Taniguchi, T.; Kadowaki, H.; Takatsu, H.; Fåk, B.; Ollivier, J.; Yamazaki, T.; Sato, T. J.; Yoshizawa, H.; Shimura, Y.; Sakakibara, T.; Hong, T.; Goto, K.; Yaraskavitch, L. R.; Kycia, J. B. Long-range order and spin-liquid states of polycrystalline $Tb_{2+x}Ti_{2-x}O_{7+y}$. *Phys. Rev. B* **2013**, *87*, 060408.
(33) Ruminy, M.; Bovo, L.; Pomjakushina, E.; Haas, M. K.; Stuhr, U.; Cervellino, A.; Cava, R. J.; Kenzelmann, M.; Fennell, T. Sample independence of magnetoelastic excitations in the rare-earth pyrochlore $Tb_2Ti_2O_7$. *Phys. Rev. B* **2016**, *93*, 144407.
(34) Shafieizadeh, Z.; Xin, Y.; Koohpayeh, S. M.; Huang, Q.; Zhou, H. Superdislocations and point defects in pyrochlore $Yb_2Ti_2O_7$ single crystals and implication on magnetic ground states. *Sci. Rep.* **2018**, *8*, 17202.
(35) Ghasemi, A.; Scheie, A.; Kindervater, J.; Koohpayeh, S. M. The pyrochlore $Ho_2Ti_2O_7$: Synthesis, crystal growth, and stoichiometry. *J. Cryst. Growth* **2018**, *500*, 38−43.
(36) Mullens, B. G.; Zhang, Z.; Avdeev, M.; Brand, H. E. A.; Cowie, B. C. C.; D'Angelo, A.; Saura Múzquiz, M.; Kennedy, B. J. Average and local ordering of $Yb_2(Ti_{2-x}Yb_x)O_{7-x/2}$ 'stuffed' pyrochlores: The development of a robust structural model. *J. Solid State Chem.* **2021**, *302*, 122412.
(37) Arpino, K. E.; Trump, B. A.; Scheie, A. O.; McQueen, T. M.; Koohpayeh, S. M. Impact of stoichiometry of $Yb_2Ti_2O_7$ on its physical properties. *Phys. Rev. B* **2017**, *95*, 094407.
(38) Mostaed, A.; Balakrishnan, G.; Lees, M. R.; Yasui, Y.; Chang, L.-J.; Beanland, R. Atomic structure study of the pyrochlore $Yb_2Ti_2O_7$ and its relationship with low-temperature magnetic order. *Phys. Rev. B* **2017**, *95*, 094431.
(39) Revell, H. M.; Yaraskavitch, L. R.; Mason, J. D.; Ross, K. A.; Noad, H. M. L.; Dabkowska, H. A.; Gaulin, B. D.; Henelius, P.; Kycia, J. B. Evidence of impurity and boundary effects on magnetic monopole dynamics in spin ice. *Nat. Phys.* **2013**, *9*, 34−37.
(40) Mullens, B. G.; Zhang, Z.; Avdeev, M.; Brand, H. E. A.; Cowie, B. C. C.; Saura Múzquiz, M.; Kennedy, B. J. Effect of long- and short-range disorder on the oxygen ionic conductivity of $Tm_2(Ti_{2-x}Tm_x)O_{7-x/2}$ "stuffed" pyrochlores. *Inorg. Chem.* **2021**, *60*, 4517−4530.
(41) Blundred, G. D.; Bridges, C. A.; Rosseinsky, M. J. New oxidation states and defect chemistry in the pyrochlore structure. *Angew. Chem., Int. Ed.* **2004**, *43*, 3562−3565.
(42) Lau, G. C.; Muegge, B. D.; McQueen, T. M.; Duncan, E. L.; Cava, R. J. Stuffed rare earth pyrochlore solid solutions. *J. Solid State Chem.* **2006**, *179*, 3126−3135.


https://doi.org/10.1021/acs.chemmater.3c02603
Chem. Mater. 2024, 36, 2325−2333

(43) Lau, G. C.; McQueen, T. M.; Huang, Q.; Zandbergen, H. W.; Cava, R. J. Long- and short-range order in stuffed titanate pyrochlores. *J. Solid State Chem.* **2008**, *181*, 45−50.
(44) Bovo, L.; Rouleau, C. M.; Prabhakaran, D.; Bramwell, S. T. Layer-by-layer epitaxial thin films of the pyrochlore $Tb_2Ti_2O_7$. *Nanotechnology* **2017**, *28*, 055708.
(45) Wen, F.; Wu, T.-C.; Liu, X.; Terilli, M.; Kareev, M.; Chakhalian, J. Epitaxial stabilization of (111)-oriented frustrated quantum pyrochlore thin films. *J. Appl. Phys.* **2021**, *129*, 025302.
(46) Kermarrec, E.; Maharaj, D. D.; Gaudet, J.; Fritsch, K.; Pomaranski, D.; Kycia, J. B.; Qiu, Y.; Copley, J. R. D.; Couchman, M. M. P.; Morningstar, A. O. R.; Dabkowska, H. A.; Gaulin, B. D. Gapped and gapless short-range-ordered magnetic states with (1/2, 1/2, 1/2) wave vectors in the pyrochlore magnet $Tb_{2+x}Ti_{2-x}O_{7+\delta}$. *Phys. Rev. B* **2015**, *92*, 245114.
(47) Honke, T.; Fujioka, H.; Ohta, J.; Oshima, M. InN epitaxial growths on yttria stabilized zirconia (111) step substrates. *J. Vac. Sci. Technol. A* **2004**, *22*, 2487−2489.
(48) Sun, J.; Parzyck, C. T.; Lee, J. H.; Brooks, C. M.; Kourkoutis, L. F.; Ke, X.; Misra, R.; Schubert, J.; Hensling, F. V.; Barone, M. R.; et al. Canonical approach to cation flux calibration in oxide molecular-beam epitaxy. *Phys. Rev. Mater.* **2022**, *6*, 033802.
(49) Nelson, J. B.; Riley, D. P. An experimental investigation of extrapolation methods in the derivation of accurate unit-cell dimensions of crystals. *Proc. Phys. Soc.* **1945**, *57*, 160−177.
(50) Cueva, P.; Hovden, R.; Mundy, J. A.; Xin, H. L.; Muller, D. A. Data processing for atomic resolution electron energy loss spectroscopy. *Microsc. Microanal.* **2012**, *18*, 667−675.
(51) Guitteny, S.; Robert, J.; Bonville, P.; Ollivier, J.; Decorse, C.; Steffens, P.; Boehm, M.; Mutka, H.; Mirebeau, I.; Petit, S. Anisotropic propagating excitations and quadrupolar effects in $Tb_2Ti_2O_7$. *Phys. Rev. Lett.* **2013**, *111*, 087201.
(52) Haaland, D. M.; Jones, H. D.; Van Benthem, M. H.; Sinclair, M. B.; Melgaard, D. K.; Stork, C. L.; Pedroso, M. C.; Liu, P.; Brasier, A. R.; Andrews, N. L.; Lidke, D. S. Hyperspectral confocal fluorescence imaging: Exploring alternative multivariate curve resolution approaches. *Appl. Spectrosc.* **2009**, *63*, 271−279.
(53) Kourkoutis, L. F.; Xin, H. L.; Higuchi, T.; Hotta, Y.; Lee, J. H.; Hikita, Y.; Schlom, D. G.; Hwang, H. Y.; Muller, D. A. Atomic-resolution spectroscopic imaging of oxide interfaces. *Philos. Mag.* **2010**, *90*, 4731−4749.
(54) Lau, G. C.; Freitas, R. S.; Ueland, B. G.; Muegge, B. D.; Duncan, E. L.; Schiffer, P.; Cava, R. J. Zero-point entropy in stuffed spin-ice. *Nat. Phys.* **2006**, *2*, 249−253.


https://doi.org/10.1021/acs.chemmater.3c02603
*Chem. Mater.* 2024, 36, 2325−2333